



## ORIGINAL ARTICLE

# Green supported Cu nanoparticles on modified Fe<sub>3</sub>O<sub>4</sub> nanoparticles using *thymbra spicata* flower extract: Investigation of its antioxidant and the anti-human lung cancer properties



Xiaoli Tang<sup>a,1</sup>, Xuelian Li<sup>b,1</sup>, Zhaodong Sun<sup>a,\*</sup>

<sup>a</sup> Department of Laboratory Medicine, The First People's Hospital of Lianyungang City, Lianyungang City, Jiangsu Province 222002, People's Republic of China

<sup>b</sup> Department of Laboratory Medicine, The Fourth People's Hospital of Lianyungang City, Lianyungang City, Jiangsu Province 222002, People's Republic of China

Received 23 January 2022; accepted 23 February 2022

Available online 1 March 2022

## KEYWORDS

Magnetic composite;  
Fe<sub>3</sub>O<sub>4</sub>/Thyme-Cu;  
Antioxidant;  
Human lung cancer

**Abstract** In recent days, the green synthesized nanomagnetic biocomposites have been evolved with tremendous potential as the future biological agents. This has encouraged us to design and synthesis of a novel Cu NPs supported *Thyme* flower extract modified magnetic nanomaterial (Fe<sub>3</sub>O<sub>4</sub>/Thyme-Cu). It was meticulously characterized using advanced analytical techniques like FT-IR, FESEM, TEM, EDX, VSM, XRD and ICP-OES. After the characterization, the synthesized Fe<sub>3</sub>O<sub>4</sub>/Thyme-Cu nanocomposite was engaged in biological assays like study of anti-oxidant properties by DPPH mediated free radical scavenging test using BHT as a reference molecule. Thereafter, on having a significant IC50 value in radical scavenging assay, we extended the bio-application of the desired nanocomposite in anticancer study of A549, Calu6 and H358 human lung cell lines in-vitro through MTT assay. They had very low cell viability and high anti-human lung cancer activities dose-dependently against A549, Calu6 and H358 cell lines without any cytotoxicity on the normal cell line (MRC-5). The IC50 of Fe<sub>3</sub>O<sub>4</sub>/Thyme-Cu nanocomposite was 124, 265, and 181 μg/mL against A549, Calu6 and H358 cell lines, respectively. Maybe significant

\* Corresponding author.

E-mail address: [lindery001@sina.com](mailto:lindery001@sina.com) (Z. Sun).

<sup>1</sup> Xiaoli Tang and Xuelian Li contributed equally to the article.

Peer review under responsibility of King Saud University.



anti-human lung cancer potentials of Fe<sub>3</sub>O<sub>4</sub>/Thyme-Cu nanocomposite against common lung cancer cell lines are related to their antioxidant activities. So, these results suggest that synthesized Fe<sub>3</sub>O<sub>4</sub>/Thyme-Cu nanocomposite as a chemotherapeutic nanomaterial have a suitable anticancer activity against lung cell lines.

© 2022 The Authors. Published by Elsevier B.V. on behalf of King Saud University. This is an open access article under the CC BY-NC-ND license (<http://creativecommons.org/licenses/by-nc-nd/4.0/>).

## 1. Introduction

In the era of advanced functional materials noble metal nanoparticles (NPs) have garnered substantial importance derived from their distinctive physicochemical properties. Due to minuscule dimension they acquire large surface to volume ratio, which is greatly responsible for their high catalytic activity (Vinci and Rapa, 2019; Habibullah et al., 2021; Pareek et al., 2017; Dauthal and Mukhopadhyay, 2016; Bao and Lan, 2019; Pradeep, 2009; Conde et al., 2012). Among the different noble metal NPs (Au, Ag, Cu, Hg, Pd, Pt) Cu NP are significantly interesting which has been found very stable both physically and chemically and also much economic among the all (Gawande et al., 2016; Singh and Kaur, 2016). They can be prepared in various morphologies like nanospheres, nanorods, nanocubes, nanostars, nanoflowers, nanowires, nanorice etc. Due to unique shape selective physical properties, Cu NPs have profuse applications in diverse scientific domains like physics, chemistry, biology, material science, medicines and their interdisciplinary subjects (Al-Hakkani and Appl, 2020; Waris et al., 2021; Bhagat et al., 2021; Chakraborty et al., 2022; Din et al., 2017). Nevertheless, these NPs when being used barely in different applications, especially in catalysis, tend to agglomerate and the activity gets reduced abruptly. Again, there also difficulty lies in the isolation of catalyst from reaction medium due to its tiny size. These difficulties however can be turned aside by immobilization of the NPs over a suitable support that prevents them to coalesce together (Veisi et al., 2021; Hemmati et al., 2020). Now, with reference to stability of NPs by successful dispersion over the support and facile isolation, magnetic nanoparticles (MNP) as a support matrix, have garnered special priority. In addition, they are bestowed with plenteous hydroxyl groups on the exterior that could be exploited to appropriate surface modifications. The material is inexpensive, readily available, easy to synthesize, having exceptional thermal and mechanical stability, being non-hazardous and biocompatible (Naghypour and Fakhri, 2016; Duan et al., 2018; Veisi et al., 2018; Pinto et al., 2012; Mahasti et al., 2019; Maia et al., 2019; Veisi et al., 2021; Shahriari et al., 2021).

Presently, advanced bio-engineered nanomaterials derived from natural resources have come with great prominence in catalysis as well as bio-applications due to their unique sustainable features like biocompatibility, biodegradability, reusability, uniform shape distribution and site selective physicochemical properties (Hutchison, 2008; Varma, 2014). In this regard, different plant extracts (fruit, flower, bark, seed, leaves etc) have been extensively used in the modification of nanomaterials. The resource is essentially green, easily available and economical. The organic phytochemicals contained therein are mostly electron rich oxygen or nitrogenous functions and have remarkable potential to anchor noble metal ions, reduce them to corresponding NPs in a toxic-free environment following green pathway and finally stabilizes them by capping (Mohammadinejad et al., 2016; Machado et al., 2013; Lopez-Tellez et al., 2013; Kumar et al., 2013; Kharissova et al., 2013; Sharma et al., 2015; Nadagouda et al., 2014; Sarmah et al., 2019; Vishnukumar et al., 2017; Sun et al., 2014). All these features impelled us to assemble and design a biogenic magnetic nanocomposite material Fe<sub>3</sub>O<sub>4</sub>/Thyme-Cu, where Cu NPs were synthesized *in situ* and encapsulated over Thyme phytomolecule functionalized magnetic Fe<sub>3</sub>O<sub>4</sub> NPs. The biomolecular modification over Fe<sub>3</sub>O<sub>4</sub> affords it a

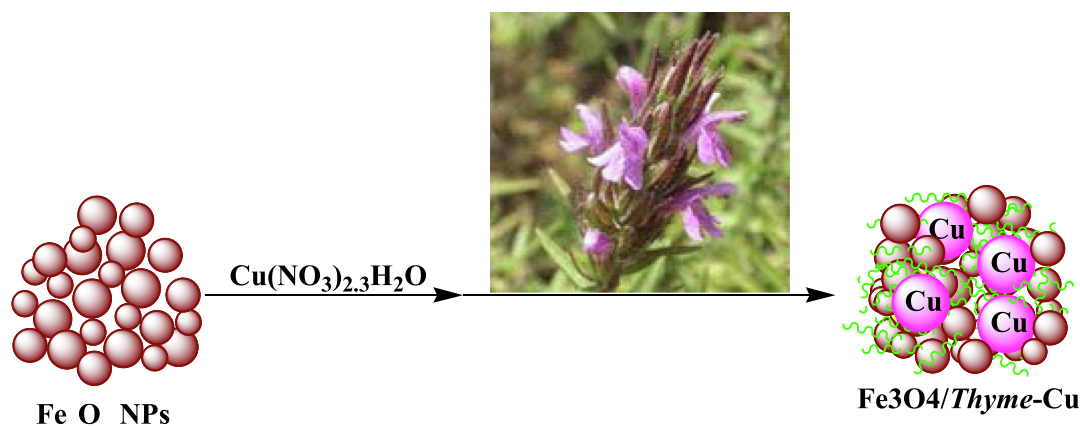
shield like appearance, more precisely, a core-shell type structure. Finally, this novel hybrid material was utilized in the biological evaluation of anti-lung cancer properties, and also the assessment of its antioxidant potential. Thyme plant (*Thymus vulgaris*) is a low-growing hardy perennial, a fragrant herb with small, fragrant leaves and thin, woody stems. The major phytochemicals active in thyme flower extract are different phenolic compounds like borneol, carvacrol, cymol, linalool, thymol, tannin, apigenin, luteolin, saponins, and triterpenic acid (Dauqan and Abdullah, 2017; Nieto, 2020).

In human body system among the different diseases cancer or malignancy is the most formidable one associated with uncontrolled growth of anomalous cells and disruption of genetic elements, affecting any part of the body (Wang et al., 2022; Huang et al., 2021). Among the different cancers, the disorderliness of lung has been the most common. Lung cancer is responsible for the second highest mortality rate worldwide owing to its severe invasion rate and metastasis. Keeping in mind of the acute side effects of conventional treatment procedures, there has been ample research on the alternate formulation of typical cancer drugs and in result nanomedicines, particularly the bio-inspired nanomaterials have come up with great prominence and potential (Ou et al., 2022; <https://www.cancer.gov/aboutcancer/understanding/what-is-cancer>). Very recently, modified Cu NPs has been explored as an excellent chemotherapeutic drug in cancer detection and inhibition of its proliferation (Huang et al., 2021; Xue et al., 2021; Shi et al., 2021; Sun et al., 2022; Tamimi et al., 2020; Yao et al., 2020). Hence, in our investigations we used the Fe<sub>3</sub>O<sub>4</sub>/Thyme-Cu nanocomposite against some standard human cancer cell lines, namely, A549, Calu6 and H358 and interestingly achieved some very good outputs inhibiting their growth. However, the material was proved benign without any significant cytotoxicity on the normal cell line (MRC-5). Again, Cu NPs and thyme extract have been observed to exhibit considerable antioxidant potential individually. Definitely, to our anticipation, the Fe<sub>3</sub>O<sub>4</sub>/Thyme-Cu material showed superior antioxidant activities.

## 2. Experimental

### 2.1. Materials and method

The essential chemicals and biosamples were procured from Fluka and Sigma-Aldrich. In the structural characterizations, FT-IR was recorded over KBr disc in a Bruker VERTEX 80v spectrophotometer. Morphological and compositional analysis was done over FE-SEM MIRA3 microscope equipped with EDX (TSCAN). The samples were coated with gold atom vapor prior to analysis. A Philips CM10 microscope was used in the TEM analysis, performed at 200 kV operating voltage. The sample was prepared by dispersing it on a carbon coated Cu grid followed by drying. In the analysis of crystallinity, X-ray diffraction study was performed using Co K $\alpha$  radiation ( $\lambda = 1.78897 \text{ \AA}$ , voltage 40 keV, current 40 mA) in the scanning range of  $2\theta = 10$  to  $80^\circ$ . A STAT FAX 2100, BioTek, Winooski, USA instrument was used in Microplate Reading [Scheme 1](#).



**Scheme 1** Green synthesis of magnetic Fe<sub>3</sub>O<sub>4</sub>/Thyme-Cu nanocomposite mediated by *Thyme* flower extract.

## 2.2. Preparation of *Thyme* flower extract

Clean *Thyme* flowers were collected and dried. 1.0 g of dried flowers were immersed into 30 mL DI water and gently warmed at 80 °C for 20 min when the solution color changed to light violet or pink. It was filtered through Whatman-1 filter paper and the filtrate was treated as extract.

## 2.3. Synthesis of the Fe<sub>3</sub>O<sub>4</sub> magnetite nanoparticles

A mixture of FeSO<sub>4</sub>·7H<sub>2</sub>O (4.2 g) and FeCl<sub>3</sub>·6H<sub>2</sub>O (6.1 g) were dissolved in DI water (100 mL) by stirring at 90 °C for 30 min followed by the dropwise addition of 10 mL anhydrous ammonia. Immediately brown colored Fe<sub>3</sub>O<sub>4</sub> NPs were formed. The mixture was continuously stirred for another 30 min under the same conditions and then the products were retrieved magnetically, washed thoroughly with DI water to neutrality and dried at 80 °C.

## 2.4. Green synthesis of the Fe<sub>3</sub>O<sub>4</sub>/Thyme-Cu nanoparticles

0.5 g Fe<sub>3</sub>O<sub>4</sub> NPs were dispersed in DI water (100 mL) by sonication for 20 min and then an aqueous solution of Cu(NO<sub>3</sub>)<sub>2</sub>·3H<sub>2</sub>O (50 mL, 2 mM) was added to the solution dropwise and stirred for 10 min. The prepared flower extract (10 mL) was subsequently added and stirred for 2 h at 100 °C. The Fe<sub>3</sub>O<sub>4</sub>/Thyme-Cu nanocomposite was finally separated using magnet, washed with DI water to remove the adhered byproducts and dried at 60 °C.

## 2.5. Antioxidant analysis

An equal volume of DPPH free radical solution (0.04 mg/mL, 150 µL) was mixed to 5 different concentrations (31.25, 62.5, 125, 250, 500 and 1000 µg/mL) of the nanocomposite and subsequently incubated for 30 min. Absorbances of the corresponding mixtures were measured at 517 nm and the following equation was used to calculate the radical scavenging activity in terms of % inhibition.

$$\text{Inhibition (\%)} = \left(1 - \frac{Abs_{\text{sample}} - Abs_{\text{blank}}}{Abs_{\text{control}} - Abs_{\text{blank}}}\right) \times 100 \quad (1)$$

*Abs sample*: absorbance of the reaction mixture, *Abs blank*: absorbance of the blank for each sample dilution in DPPH solvent, *Abs control*: absorbance of DPPH solution in sample solvent.

## 2.6. Cytotoxicity studies by MTT assay

The cell lines were initially cultured in 96-well plates at 37 °C in 5% CO<sub>2</sub> atmosphere for 24 h. The growth media (10% FBS) was then decanted off from the plate and were washed twice with PBS. The compounds were then introduced in different concentrations (0.5, 5, 50, 500, and 1000 µg/mL) in RPMI medium and the system was incubated again for 3 days. The MTT dye in PBS solution (10 µL, 5 mg/mL) was next added to each well and incubated again for 4 h. In the same way media was removed and replaced with 100 µL DMSO in each well. In order to assist the formazan crystal solubilization all the plates were gently swirled. Finally, absorbance of the resulting mixture was measured at 545 nm and % cell toxicity alongwith IC 50 were determined as the following formula.

$$\text{Toxicity\%} = \left(1 - \frac{\text{mean OD of sample}}{\text{mean OD of control}}\right) \times 100$$

$$\text{Viability\%} = 100 - \text{Toxicity\%}$$

## 3. Results and discussion

### 3.1. Characterization of Fe<sub>3</sub>O<sub>4</sub>/Thyme-Cu nanocomposite

A post-synthetic modification approach was followed in the synthesis of biogenic Cu grafted and thymine functionalized ferrite nanocomposite. Structural features of the core-shell type material were determined over a broad range of analytical techniques like FT-IR, SEM, EDX, elemental mapping, TEM and VSM. Fig. 1 represents unified FT-IR spectra of bare Fe<sub>3</sub>O<sub>4</sub>, thyme flower extract and Fe<sub>3</sub>O<sub>4</sub>/Thyme-Cu in order to compare the structural statistics and stepwise building of the final material. Fig. 1a shows the characteristic absorption peaks of Fe<sub>3</sub>O<sub>4</sub> where two important signals are observed at 442 and 582 cm<sup>-1</sup> due to Fe(O<sub>h</sub>)—O and Fe(T<sub>d</sub>)—O—Fe(O<sub>h</sub>) stretching vibrations (Fig. 1a) where O<sub>h</sub> and T<sub>d</sub> are the octahedral and tetrahedral position of the ferrite spinel. Two significant vibrational bands attributed to ferrite surface O-H

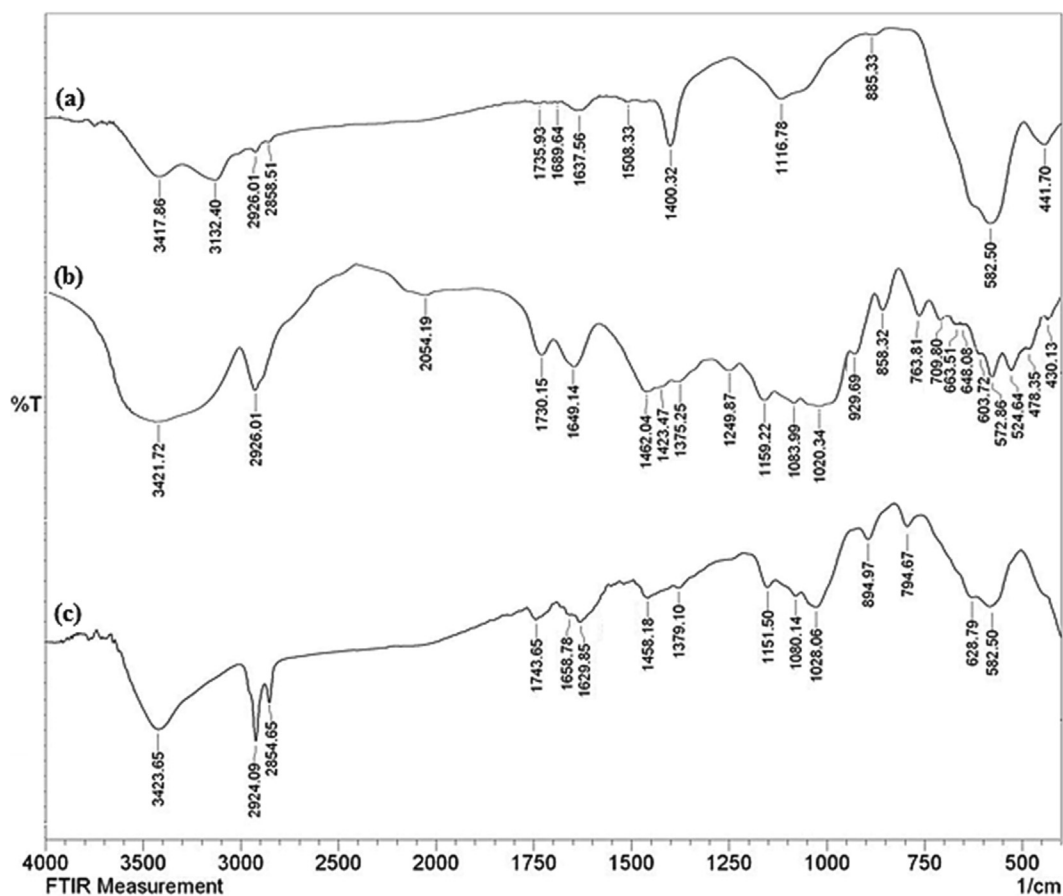


Fig. 1 The FT-IR spectra of  $\text{Fe}_3\text{O}_4$  NPs (a), *Thyme* flower extract (b) and green synthesized  $\text{Fe}_3\text{O}_4/\text{Thyme-Cu}$  (c).

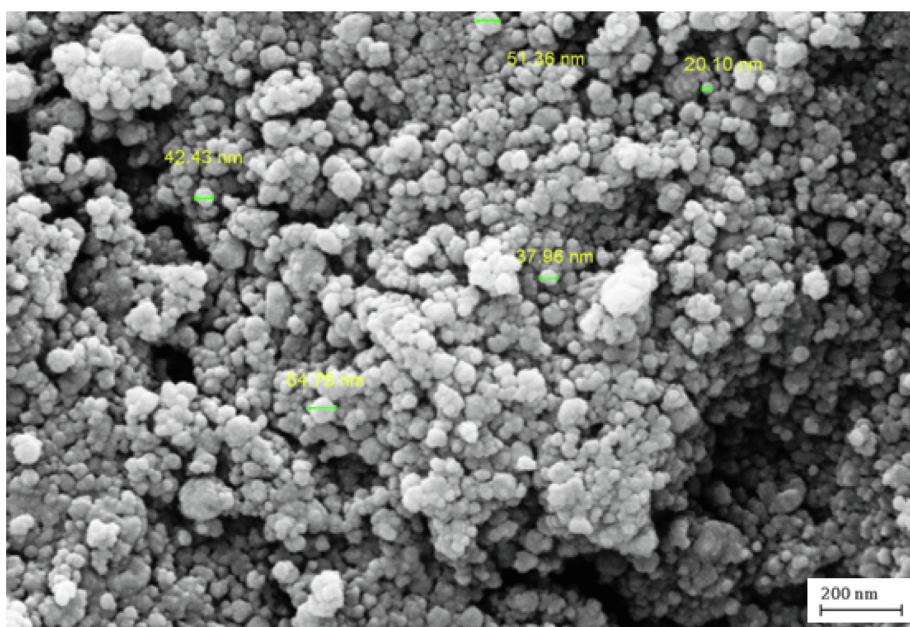
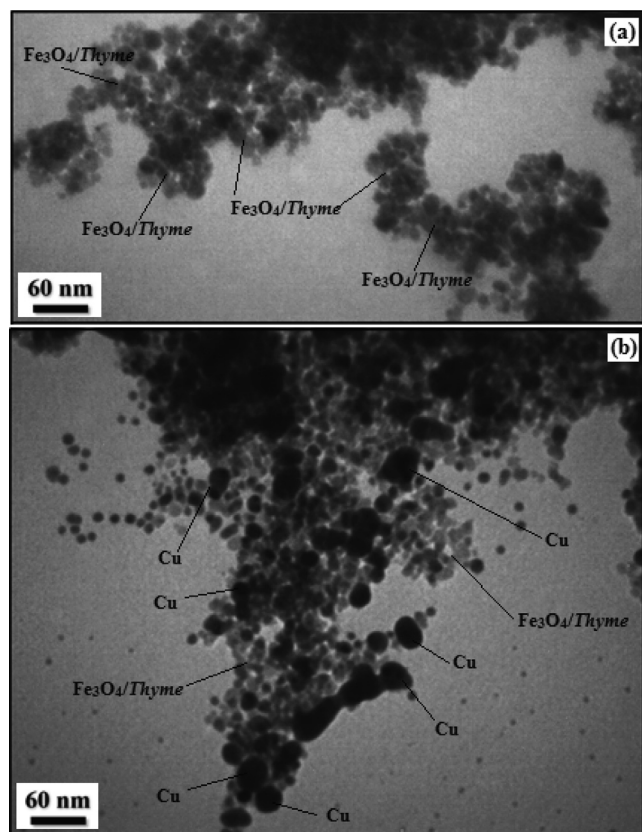


Fig. 2 SEM image of  $\text{Fe}_3\text{O}_4/\text{Thyme-Cu}$  nanocomposite.

stretching and that of intercalated  $\text{H}_2\text{O}$  molecules are found at  $3420$  and  $1638\text{ cm}^{-1}$ , respectively. As the *Thyme* flower extract contains numerous organofunctions, the corresponding FT-IR spectrum is quite complex. However, the extract is rich in phe-

nolic moieties, being evident from a broad hump at  $3422\text{ cm}^{-1}$ . Some more specific vibrations are observed at  $1076$ ,  $1421$ ,  $1650$ ,  $1730$ , and  $2926\text{ cm}^{-1}$  attributed to C–O, C–O–C, C=C, C=O and C–H stretching vibrations implying the



**Fig. 3** TEM images of (a) Fe<sub>3</sub>O<sub>4</sub>/Thyme and (b) Fe<sub>3</sub>O<sub>4</sub>/Thyme-Cu nanocomposite.

presence of flavonoid, tannin and terpenoid moieties (Fig. 1b). On the other hand, the FT-IR spectrum of Fe<sub>3</sub>O<sub>4</sub>/Thyme-Cu nanocomposite in Fig. 1c, seems to be an ensemble of the precursors, validating the successful immobilization of plant biomolecules over ferrite NPs. However, the Cu connection could be identified by the slight shifting of vibrational peaks in Fig. 1c from Fig. 1a and b.

The general microstructural features, morphology, size and shape of the as-synthesized Fe<sub>3</sub>O<sub>4</sub>/Thyme-Cu nanocomposite were ascertained by electron microscopic analysis (SEM and TEM). Fig. 2 represents the SEM image displaying the homogeneous globular morphology of the NPs. Mean particle diameter of the nanocomposite was 30–40 nm. However, plant biomolecular modification or Cu immobilization over the core

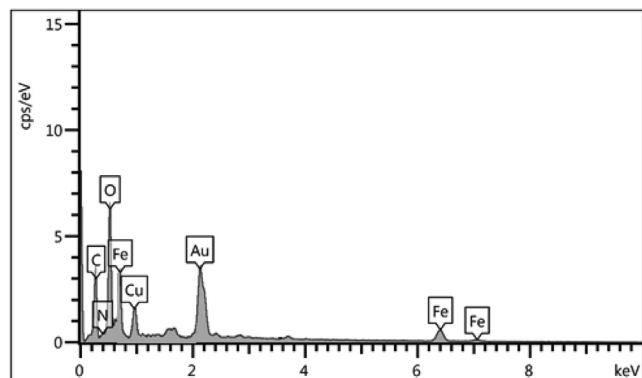


**Fig. 4** EDX spectrum of Fe<sub>3</sub>O<sub>4</sub>/Thyme-Cu nanocomposite.

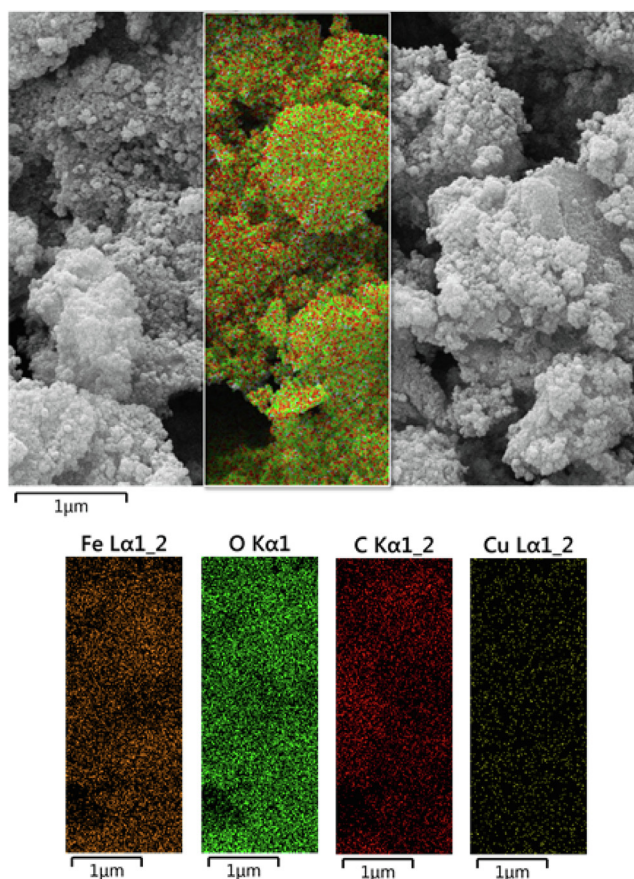


**Fig. 5** SEM image of Fe<sub>3</sub>O<sub>4</sub>/Thyme-Cu nanocomposite with its elemental mapping.

ferrite could not be separately detected from its appearances. The sample seems fairly agglomerated due to manual sample preparations prior to SEM analysis.

The structural inherence was further established by TEM analysis. Fig. 3 depicts the texture of Fe<sub>3</sub>O<sub>4</sub>/Thyme intermediate and the final Fe<sub>3</sub>O<sub>4</sub>/Thyme-Cu nanocomposite. It substantively justifies the outcomes of SEM results with globular shaped particles. Fig. 3a shows the core grey particles representing Fe<sub>3</sub>O<sub>4</sub> NPs which is associated with a continuous homogenous layer of thyme biomolecules over it. Then again Fig. 3b shows the fabrication of tiny spherical Cu NPs over Fe<sub>3</sub>O<sub>4</sub>/Thyme surface. The NPs are being stabilized over thyme phytochemicals by capping. The grey and black particles characterize the Fe<sub>3</sub>O<sub>4</sub> and Cu NPs respectively. By size the latter seems comparably larger where the corresponding dimensions being in the range of 15–20 nm and 20–30 nm respectively. It personifies a blend of the two NPs but no sign of agglomeration was detected from the image.

We got an idea of chemical constitution of the Fe<sub>3</sub>O<sub>4</sub>/Thyme-Cu nanocomposite from EDX analysis. As seen from the profile in Fig. 4, the material is composed of Fe and Cu as metallic and C, N and O as the non-metallic components. The strong signal at 2.15 keV due to Au appears as a result of gold coating over the sample prior to SEM-EDX analysis. The occurrence of non-metals authenticates the plant biomolecular attachments. EDX outcomes were further warranted by SEM elemental mapping study (Fig. 5) which demonstrates the elemental distribution or topography over

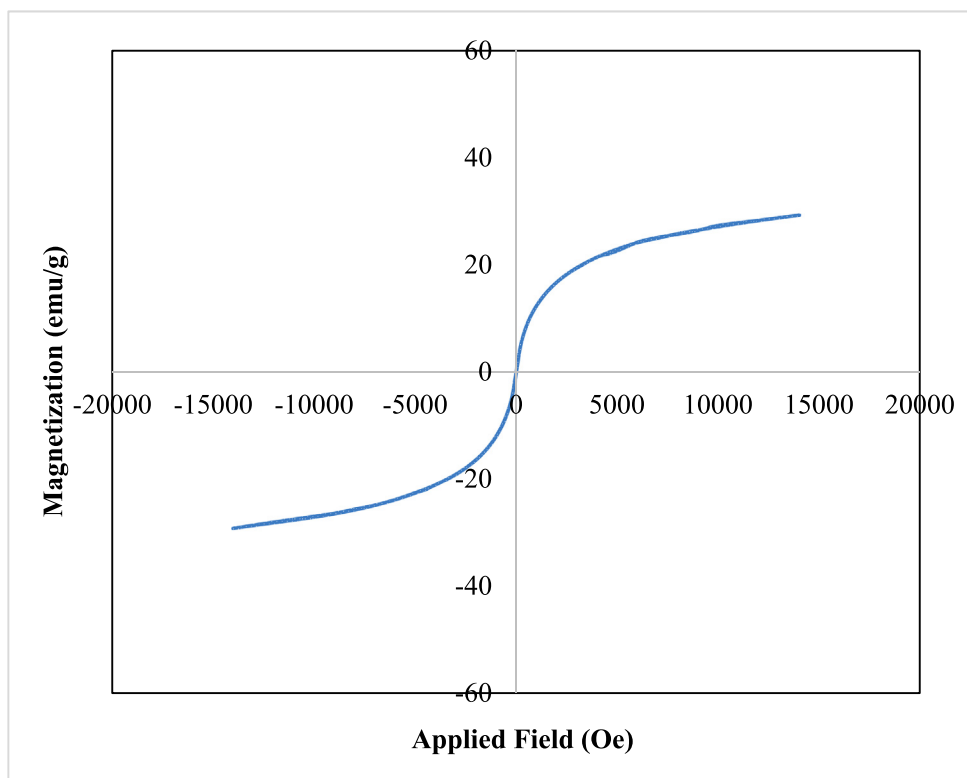


Fig. 6 VSM analysis of  $\text{Fe}_3\text{O}_4/\text{Thyme-Cu}$  nanocomposite.

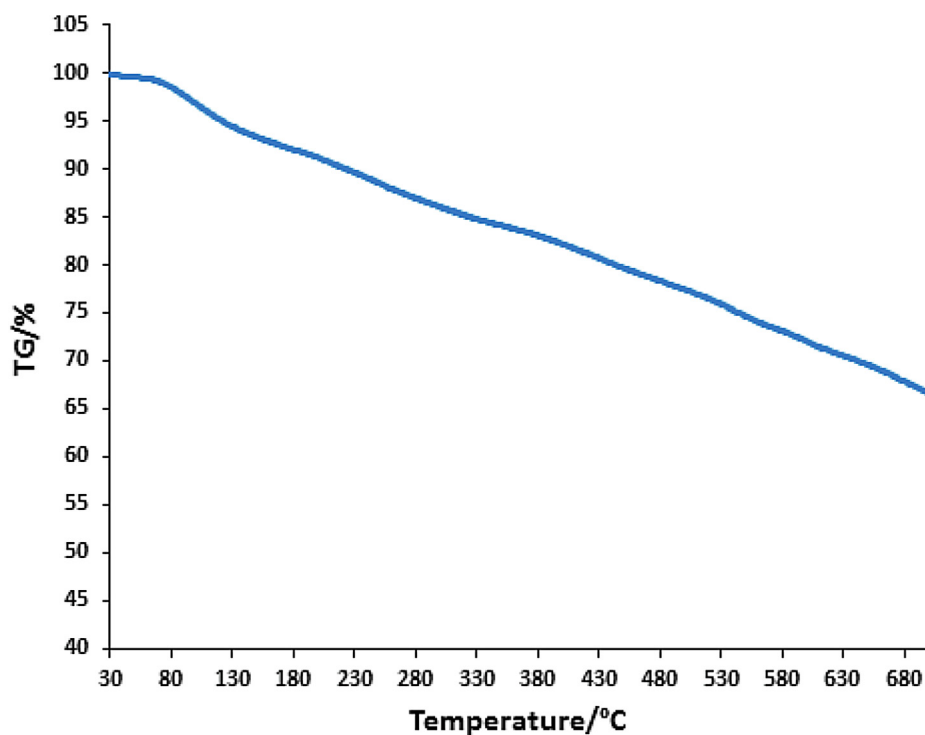
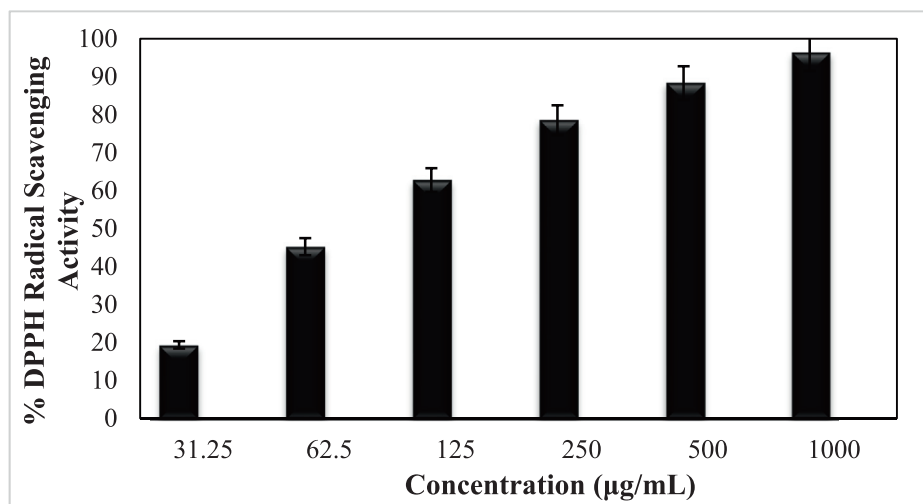


Fig. 7 TGA curve of  $\text{Fe}_3\text{O}_4/\text{Thyme-Cu}$  nanocomposite.

the matrix. Evidently, Fe, Cu, C and O species are dispersed uniformly throughout the surface. The uniform distribution of active elements definitely has an augmented impact on its activity.

Being an iron cored material, the study of magnetic properties of  $\text{Fe}_3\text{O}_4/\text{Thyme-Cu}$  by VSM is an imperative measure. By applying a magnetic field of  $-20$  kOe to  $+20$  kOe, it produces a typical magnetic hysteresis curve, justifying the material to be



**Fig. 8** Antioxidant activity of Fe<sub>3</sub>O<sub>4</sub>/Thyme-Cu nanocomposite.

superparamagnetic in nature (Fig. 6). The saturation magnetization ( $M_s$ ) value was found 23.6 emu/g. The lower magnetic value than unmodified Fe<sub>3</sub>O<sub>4</sub> can be justified due to the loading of non-magnetic Cu NPs as well as the plant biomolecules. However, the material is still enough magnetic to be attracted by an external magnet.

The stability of the Fe<sub>3</sub>O<sub>4</sub>/Thyme-Cu nanocomposite and also percent of organic groups on the magnetic NPs surface were analyzed using TGA analysis. The TGA curve (Fig. 7) shows a primary weight loss of 7.5% up to 170 °C which is because of physically adsorbed solvent and surface hydroxyl groups on the support. Thermal degradation of the nanocomposite happened following 200 °C which shows the high thermo-stability of nanocomposite. The second and third weight loss of 26.2% over the range of 200–600 °C was due to degrading the organic remains.

### 3.2. Study of antioxidant potential of Fe<sub>3</sub>O<sub>4</sub>/Thyme-Cu nanocomposite

NPs are reported to have distinctive antioxidant properties (Katata-Seru et al., 2018). When plant extracts are being

functionalized over metal NPs as capping agents, the as-synthesized nanocomposites exhibit much superior antioxidant effects. Antioxidants are generally referred to as substances that can delay, slow down, and even stop oxidation processes (Mou et al., 2015; Will et al., 2006; Harada et al., 2007; Schroeder et al., 2012; Gobbo et al., 2015). These compounds can optimally prevent changes in the color and taste of food because of oxidation reactions. They actually prevent the spread of oxidation chain reactions by releasing hydrogen atoms or electrons to free radicals. In recent years, the use of synthetic antioxidants like BHT, BHA, TBHQ as well as other chemical additives has been limited due to their potential toxicity and carcinogenicity. Therefore, scientific communities are engaged in serious research to introduce newly formulated bio-inspired and safe antioxidants derived from plant, animal, microbial and food sources (Sankar et al., 2014). In this study, we have demonstrated the radical scavenging capacity of Fe<sub>3</sub>O<sub>4</sub>/Thyme-Cu nanocomposite using DPPH radical using aqueous methanol (1:1) and BHT as negative and positive controls respectively. During scavenging the DPPH free radical, Fe<sub>3</sub>O<sub>4</sub>/Thyme-Cu transfers an electron or hydrogen to it and

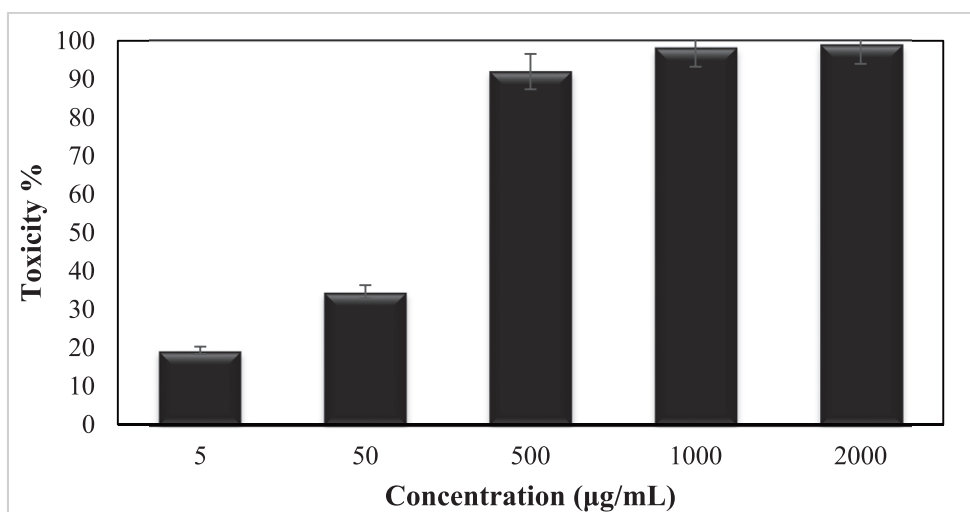


**Fig. 9** In vitro toxicity analysis of Fe<sub>3</sub>O<sub>4</sub>/Thyme-Cu nanocomposite on A549 cell line.

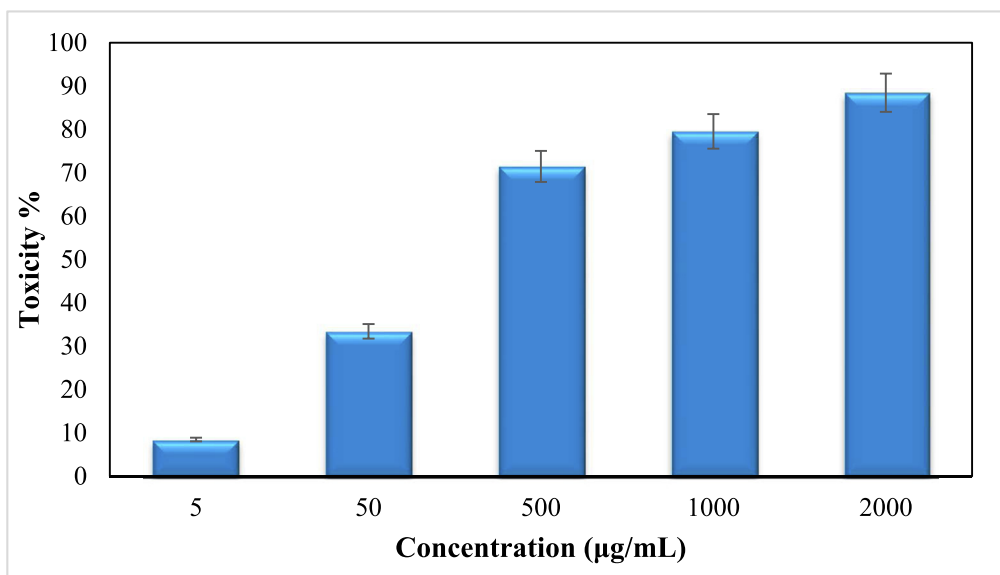


**Fig. 10** *In vitro* toxicity analysis of  $\text{Fe}_3\text{O}_4/\text{Thyme}$ -Cunanocomposite on Calu6 cell line.

reduces the radical to a stable molecular species, resulting a change of color from initial deep purple to pale yellow. This change was measured thorough UV-Vis spectroscopy at 517 nm and the corresponding antioxidant properties were calculated following Eq. (1) and expressed as percentage inhibition. UV absorbances (A) of the nanocomposite-DPPH complex at different concentrations were measured (31.25, 62.5, 125, 250, 500 and 1000 µg/mL) and the outcome as been shown in Fig. 8. Evidently, the activity got enhanced with higher concentrations and became highest (92%) at 1000 µg/mL.

### 3.3. Cytotoxicity studies over $\text{Fe}_3\text{O}_4/\text{Thyme}$ -Cu nanocomposite.

Advanced nanomaterials have a significant ability to destroy cancer or malignant cells by irradiation, providing a micro-

scopic therapeutic effect within electrons (Pascal et al., 1999; Bomati-Miguel et al., 2008; Khanna et al., 2018; Xie et al., 2018). They are designed to achieve optimal therapeutic efficacy against the cancer cells. After having a significant IC50 value in the radical scavenging study in the antioxidant assay, we further explored the  $\text{Fe}_3\text{O}_4/\text{Thyme}$ -Cu nanocomposite in the anti lung cancer study over three standard cell lines, such as, A549, Calu6 and H358 *in vitro* conditions. In the cytotoxicity measurement the cells were treated in different concentrations of the nanocomposite (5–2000 µg/mL) and were investigated by MTT assay for 48 h. Interestingly, the % cell viability values over the cancer cell lines reduced with increasing doses of  $\text{Fe}_3\text{O}_4/\text{Thyme}$ -Cu (Figs. 9–11). The corresponding IC50 values over the three cell lines were 124.28, 265.23 and 181.34 µg/mL respectively. The cytotoxicity study was also carried on normal MRC-5 cell line which however showed

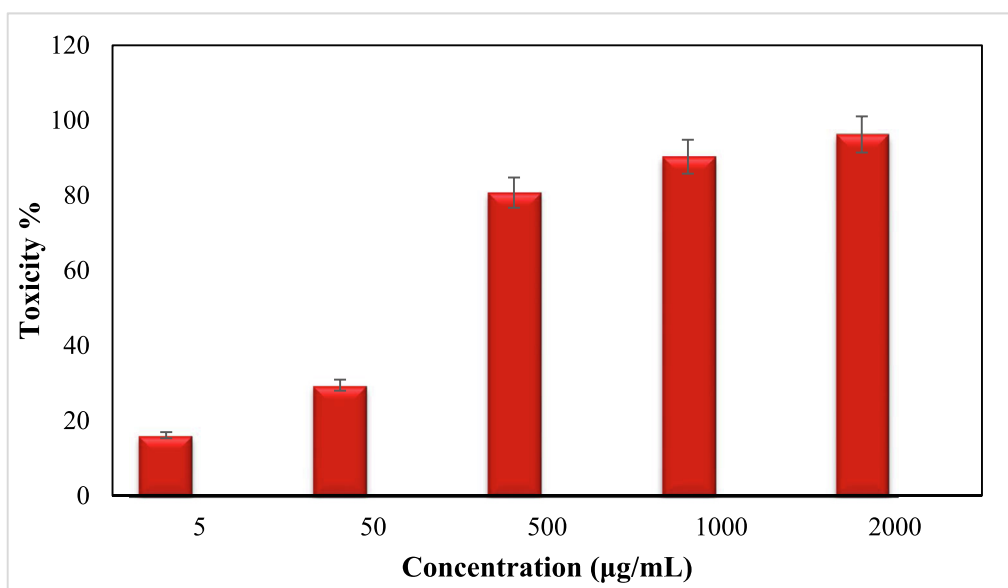


**Fig. 11** *In vitro* toxicity analysis of  $\text{Fe}_3\text{O}_4/\text{Thyme}$ -Cu nanocomposite on H358 cell line.

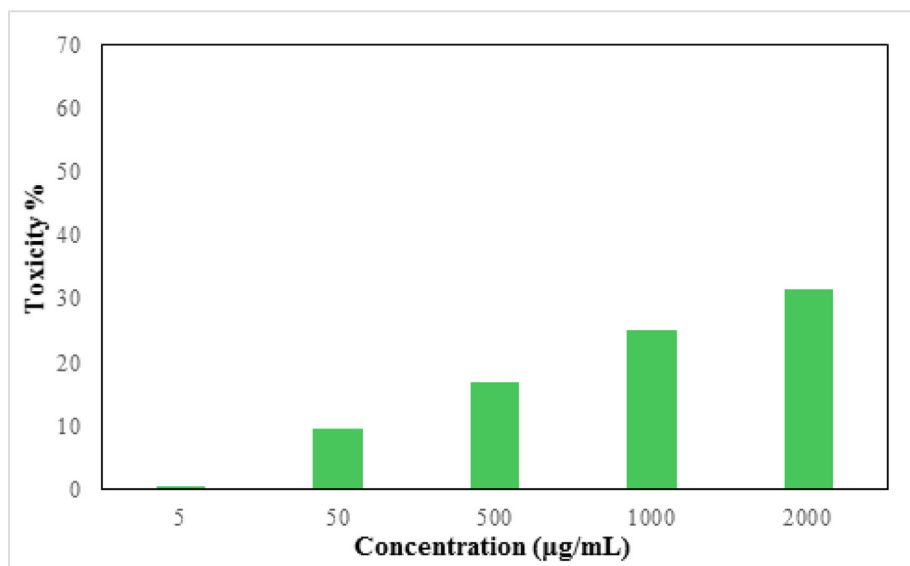


Fig. 12 In vitro toxicity analysis of Fe<sub>3</sub>O<sub>4</sub>/Thyme-Cu nanocomposite on the normal cell line (MRC-5).

insignificant % cell viability as can be seen in Fig. 12 (IC<sub>50</sub> = 3132.57). Therefore, Fe<sub>3</sub>O<sub>4</sub>/Thyme-Cu definitely could play as an efficient chemotherapeutic material against the lung cancer cell lines.

#### 4. Conclusion

In summary, we demonstrate herein the design of a sustainable bio-inspired system for the synthesis of *Thymus vulgaris* flower extract modified Cu NPs, fabricated over magnetic Fe<sub>3</sub>O<sub>4</sub> NPs. The electron rich oxygenated and nitrogenous phytochemicals facilitate the toxic chemicals free green reduction of incoming Cu<sup>+2</sup> ions into corresponding NPs and further stabilizes them by capping them and checks from possible coalescence. The material was characterized by diverse analytical methods. The electron microscopic images confirmed the round shaped Cu and Fe<sub>3</sub>O<sub>4</sub> particles with their mean dimension of 15–20 and 20–30 nm respectively. The material was explored biologically in the inhibition of lung cancer cells over A549, Calu6 and H358 cell lines with some outstanding results. However, there was no significant effect on the normal MRC-5 cell lines. Prior to cancer studies, antioxidant potential of the material was determined by DPPH radical scavenging, which exhibited almost 94% activity at a dose of 1000 µg/mL. Cytotoxicity studies were performed with standard MTT assay. % Cell viability over the cell lines reduced dose-dependently over the nanocomposite and the corresponding IC<sub>50</sub> values were observed to be 124.28, 265.23 and 181.34 µg/mL respectively, whereas that over the normal cell line being a staggering 3132.57 µg/mL. The stupendous outcomes exhibited by Fe<sub>3</sub>O<sub>4</sub>/Thyme-Cu nanocomposite corroborate it as a potential formulation of chemotherapeutic drug in lung cancer management.

#### References

- Vinci, G., Rapa, M., 2019. *Bioengineering (Basel)*. 6 (1), 10.
- Habibullah, H., Viktorova, J., Ruml, T., 2021. *Nanoscale Res. Lett.* 16, 47.
- Pareek, V., Bhargava, A., Gupta, R., Jain, N., Panwar, J., 2017. *Adv. Sci. Eng. Med.* 9 (7), 527–544.
- Dauthal, P., Mukhopadhyay, M., 2016. *Ind. Eng. Chem. Res.* 55 (36), 9557–9577.
- Bao, Z., Lan, C.Q., 2019. *Colloids Surf. B: Biointerfaces* 184, 110519.
- Pradeep, T., Anshup, 2009. *Thin Solid Films* 517 (24), 6441–6478.
- Conde, J., Doria, G., Baptista, P., 2012. *J. Drug Delivery* 751075.
- Gawande, M.B., Goswami, A., Felpin, F.-X., Asefa, T., Huang, X., Silva, R., Zou, X., Zboril, R., Verma, R.S., 2016. *Chem. Rev.* 116 (6), 3722–3811.
- Singh, J., Kaur, G., 2016. *J. Bioelectron. Nanotechnol.* 1 (1), 9.
- Al-Hakkani, M.F., 2020. *Appl. Sci.* 2, 505.
- Waris, A., Din, M., Ali, A., Ali, M., Afridi, S., Baset, A., Khan, A.U. 2021, *Inorg. Chem. Commun.* 123 108369; (b) Rezaeati, S. Ramazani, A., Sajjadifar, S., Aghahosseini, H., Rezaei, A., 2021. *ACS Omega*, 6 39 25608-25622; (c) Rezaeati, S., Kalantari, F., Ramazani, A., Sajjadifar, S., Aghahosseini, H., Rezaei, A., 2022. *Inorganic Chem.* 61 2, 992-1010; (d) Nakhaei, A., Davoodnia, A., Nakhaei, H., 2019. *J. Chem. Rev.*, 139-153; (e) Hamelian, M., Varmira, K., Veisi, H., 2018. *J. Photochem. Photobiol. B: Biol.* 184 71-79; (f) Lotfi, S., Veisi, H., 2019. *Mater. Sci. Eng.: C* 105 110112; (g) Mirfakhraei, S., Hekmati, M., Eshbala, F.H., Veisi, H., 2018. *New J. Chem.* 42 1757-1761; (h) Veisi, H., Ebrahimi, Z., Karmakar, B., Tamoradi, T., Ozturk, T., 2022. *Int. J. Biol. Macromol.* 200, 132.
- Bhagat, M., Anand, R., Sharma, P., Rajput, P., Sharma, N., Singh, K., 2021. *J. Solid State Sci. Technol.* 10, 063011.
- (a) Chakraborty, N., Banerjee, J., Chakraborty, P., Banerjee, A., Chanda, S., Ray, K., Acharya, K., Sarkar, J., 2022. *Green Chem. Lett. Rev.* 15 185-213; (b) Gao, G., Di, J.-Q., Zhang, H.-Y., Mo, L.-P., Zhang, Z.-H., 2020. *J. Catal.*, 387 39; (c) Zhang, M., Liu, Y.-H., Shang, Z.-R., Hu, H.-C., Zhang, Z.-H., 2017. *Catal. Commun.* 88 39.
- Din, M.I., Arshad, F., Hussain, Z., Mukhtar, M., 2017. *Nanoscale Res. Lett.* 12, 638.
- (a) Veisi, H., Karmakar, B., Tamoradi, T., Tayebee, R., Sajjadifar, S., Lotfi, S., Maleki, B., Hemmati, S., 2021. *Sci. Rep.* 11 1-15; (b) Veisi, H., Kazemi, S., Mohammadi, P., Safarimehr, P., Hemmati, S., 2019. *Polyhedron* 157, 232-240.
- Hemmati, S., Heravi, M.M., Karmakar, B., Veisi, H., 2020. *J. Mol. Liq.* 319, 114302.
- Naghypour, A., Fakhri, A., 2016. *Catal. Commun.* 73, 39–45.
- Duan, X., Liu, J., Hao, J., Wu, L., He, B., Qiu, Y., Zhang, J., He, Z., Xi, J., Wang, S., 2018. *Carbon* 130, 806–813.
- Veisi, H., Sarachegol, P., Hemmati, S., 2018. *Polyhedron* 156, 64–71.
- Pinto, I.S.X., Pacheco, P.H.V.V., Coelho, J.V., Lorençon, E., Ardisson, J.D., Fabris, J.D., de Souza, P.P., Krambrock, K.W.H., Oliveira, L.C.A., Pereira, M.C., 2012. *Appl. Catal. B: Environ.* 119–120, 175–182.

- Mahasti, N.N.N., Shih, Y.-J., Huang, Y.-H., 2019. *J. Taiwan Inst. Chem. Eng.* 96, 496–502.
- Maia, L.F.O., Hott, R.C., Ladeira, P.C.C., Batista, B.L., Andrade, T. G., Santos, M.S., Faria, M.C.S., Oliveira, L.C.A., Monteiro, D.S., Pereira, M.C., Rodrigues, J.L., 2019. *Chemosphere* 215, 422–431.
- Veisi, H., Joshani, Z., Karmakar, B., Tamoradi, T., Heravi, M.M., Gholami, J., 2021. *Int. J. Biol. Macromol.* 172, 104–113.
- Shahriari, M., Sedigh, M.A., Mahdavian, Y., Mahdigholizad, S., Pirhayati, M., Karmakar, B., Veisi, H., 2021. *Int. J. Biol. Macromol.* 172, 55–65.
- Hutchison, J.E., 2008. *ACS Nano* 2, 395–402.
- Varma, R.S., 2014. *Green Chem.* 16, 2027–2041.
- Mohammadinejad, R., Karimi, S., Iravani, S., Varma, R.S., 2016. *Green Chem.* 18, 20–52.
- Machado, S., Pinto, S.L., Grosso, J.P., Nouws, H.P.A., Albergaria, J. T., Delerue-Matos, C., 2013. *Sci. Total Environ.* 445, 1–8.
- Lopez-Tellez, G., Balderas-Hernandez, P., Barrera-Diaz, C.E., Vilchis-Nestor, A.R., Roa-Morales, G., Bilyeu, B., 2013. *J. Nanosci. Nanotechnol.* 13, 2354–2361.
- Kumar, K.M., Mandal, B.K., Kumar, K.S., Reddy, P.S., Sreedhar, B., 2013. *Spectrochim. Acta A* 102, 128–133.
- Kharissova, O.V., Dias, H.V.R., Kharisov, B.I., Pérez, B.O., Pérez, V. M., 2013. *J. Biotechnol.* 31, 240–248.
- Sharma, D., Kanchi, S., Bisetty, K., 2015. *Arab. J. Chem.* 12 (8), 3576–3600.
- Nadagouda, M.N., Iyanna, N., Lalley, J., Han, C., Dionysiou, D.D., Varma, R.S., 2014. *ACS Sustainable Chem. Eng.* 2, 1717–1723.
- Sarmah, M., Neog, A.B., Boruah, P.K., Das, M.R., Bharali, P., Bora, U., 2019. *ACS Omega* 4, 3329–5340.
- Vishnukumar, P., Vivekanandhan, S., Muthuramkumar, S., 2017. *ChemBioEng. Rev.* 4, 18–36.
- Sun, D., Zhang, G., Jiang, X., Huang, J., Jing, X., Zheng, Y., He, J., Li, Q., 2014. *J. Mater. Chem. A* 2, 1767–1773.
- Dauqan, E.M.A., Abdullah, A., 2017. *J. Appl. Biol. Biotechnol.* 5 (02), 17–22.
- Nieto, G., 2020. *Plants (Basel)* 9 (8), 961.
- Wang, X., Liu, Z., Bani-Fwaz, M.Z., Marzouki, R., Ali, I.H., El-kott, A.F., Alhomaid, F.A., 2022. *Arab. J. Chem.* 15, 103548.
- Huang, Y., Kang, Y., El-kott, A., Ahmed, A.E., Khames, A., Zein, M. A., 2021. *Arab. J. Chem.* 14, 103299.
- Ou, X., Karmakar, B., Awwad, N.S., Ibrahim, H.A., Osman, H.E.H., El-kott, A.F., Abdel-Daim, M.M., 2022. *Inorg. Chem. Commun.* 137, 109221.
- <https://www.cancer.gov/aboutcancer/understanding/what-is-cancer>
- Xue, W., Yang, G., Karmakar, B., Gao, Y., 2021. *Arab. J. Chem.* 14, 103306.
- Shi, Z., Mahdavian, Y., Mahdavian, Y., Mahdigholizad, S., Irani, P., Karimian, M., et al, 2021. *Arab. J. Chem.* 14, 103224.
- Sun, W., Karmakar, B., Ibrahim, H.A., Awwad, N.S., El-kott, A.F., 2022. *Arab. J. Chem.* 15, 103465.
- Tamimi, S.A., Ashraf, S., Abdulrehman, T., Parray, A., Mansour, S. A., Haik, Y., Qadri, S., 2020. *Cancer Nano* 11, 13.
- Yao, Y., Zhou, Y., Liu, L., Xu, Y., et al, 2020. *Front. Mol. Biosci.* 7, 193.
- Katata-Seru, L., Moremedi, T., Aremu, O.S., et al, 2018. *J. Mol. Liq.* 256, 296–304.
- Mou, X., Ali, Z., Li, S., He, N., 2015. *J. Nanosci. Nanotechnol.* 15 (1), 54–62.
- Will, S., Purkayastha, C., Chan, C., et al, 2006. *Lancet Oncol.* 7 (1), 52–60.
- Harada, T., Tanigawa, N., Matsuki, M., Nohara, T., Narabayashi, I., 2007. *Eur. J. Radiology* 63 (3), 401–407.
- Schroeder, A., Heller, D.A., Winslow, M.M., et al, 2012. *Nat. Rev. Cancer* 12 (1), 39–50.
- Gobbo, L., Sjaastad, K., Radomski, M.W., Volkov, Y., Prina-Mello, A., 2015. *Theranostics* 5 (11), 1249–1263.
- Sankar, R., Maheswari, R., Karthik, S., et al, 2014. *Mater. Sci. Eng. C* 44, 234–239.
- Pascal, C., Pascal, J.L., Favier, F., Moubtassim, M.L.E., Payen, C., 1999. *Chem. Mater.* 11, 141.
- Bomatí-Miguel, O., Mazeina, L., Navrotsky, A., Veintemillas-Verdaguer, S., 2008. *Chem. Mater.* 20, 591.
- Khanna, L., Verma, N.K., Tripathi, S.K., 2018. *J. Alloys Compd.* 752, 332–353.
- Xie, W., Guo, Z., Gao, F., Gao, Q., Wang, D., Liaw, B.S., Cai, Q., Sun, X., Wang, X., Zhao, L., 2018. *Theranostics* 8, 3284–3307.